J Supercond Nov Magn (2013) 26:2867–2871
DOI 10.1007/s10948-013-2264-7

ORIGINAL PAPER

Multiple Andreev Reflections Spectroscopy of Two-Gap 1111- and 11 Fe-Based Superconductors

Y.G. Ponomarev · S.A. Kuzmichev · T.E. Kuzmicheva · M.G. Mikheev · M.V. Sudakova · S.N. Tchesnokov · O.S. Volkova · A.N. Vasiliev · V.M. Pudalov · A.V. Sadakov · A.S. Usol'tsev · T. Wolf · E.P. Khlybov · L.F. Kulikova

Received: 2 May 2013 / Accepted: 8 May 2013 / Published online: 31 May 2013

Abstract Using the "break-junction" technique, we prepared and studied superconductor–constriction–superconductor (ScS) nanocontacts in polycrystalline samples of Fe-based superconductors $CeO_{0.88}F_{0.12}FeAs$ (Ce-1111; $T_C^{\rm bulk} = 41 \pm 1$ K), $LaO_{0.9}F_{0.1}FeAs$ (La-1111; $T_C^{\rm bulk} = 28 \pm 1$ K), and FeSe ($T_C^{\rm bulk} = 12 \pm 1$ K). We detected two subharmonic gap structures related with multiple Andreev reflections, indicating the presence of two superconducting gaps with the BCS-ratios $2\Delta_L/k_BT_C = 4.2 \div 5.9$ and $2\Delta_S/k_BT_C \sim 1 \ll 3.52$, respectively. Temperature dependences of the two gaps $\Delta_{L,S}(T)$ in FeSe indicate a k-space proximity effect between two superconducting condensates. For the studied iron-based superconductors, we found a linear relation between the gap Δ_L and magnetic resonance energy, $E_{\rm res} \approx 2\Delta_L$.

Keywords Fe-based superconductors · Two-gap superconductivity · Multiple Andreev reflections · Subharmonic gap structure · Break-junction

Y.G. Ponomarev · S.A. Kuzmichev · T.E. Kuzmicheva (✉) · M.G. Mikheev · M.V. Sudakova · S.N. Tchesnokov · O.S. Volkova · A.N. Vasiliev
Lomonosov Moscow State University, 119991 Moscow, Russia
e-mail: kute@lebedev.ru

T.E. Kuzmicheva · V.M. Pudalov · A.V. Sadakov · A.S. Usol'tsev
Lebedev Physical Institute RAS, 119991 Moscow, Russia

T. Wolf
Karlsruher Institut für Technologie, Institut für Festkörperphysik, 76021 Karlsruhe, Germany

E.P. Khlybov · L.F. Kulikova
Institute for High Pressure Physics RAS, 142190 Troitsk, Russia

1 Introduction

Andreev spectroscopy [1] is a powerful instrument to measure superconducting gap in a wide temperature range, up to T_C [2–4]. A number of such measurements have been performed earlier with oxypnictides of the $RFeAsO_{1-x}F_x$ family and with FeSe [5–8]. Here, we present systematic studies of the current-voltage characteristics (CVCs) and dynamic conductance $dI(V)/dV$ for superconductor–constriction–superconductor (ScS) contacts in Ce-1111, La-1111, and FeSe. Using the intrinsic multiple Andreev reflections effect (IMARE) spectroscopy, we measured the two superconducting gap values in all three Fe-based materials and determined temperature dependences of the two gaps for FeSe.

The compounds under study belong to the class of iron-based superconductors discovered in 2008 [9]. These materials are characterized by a layered crystal structure; their electron energy spectrum in the normal state contains electron and hole quasi two-dimensional Fermi surface sheets, where two superconducting condensates are supposed to be formed at $T < T_C$ [5].

2 Experimental Details

To measure the superconducting gaps, we used two methods: (i) Andreev spectroscopy [1] of single superconductor–constricition–superconductor (ScS) nanocontacts [2], and (ii) IMARE spectroscopy of ScS-contact stacks. The nanosized contacts required for multiple Andreev reflections spectroscopy have been made using the "break-junction" technique [10]. In this technique, breaking a bulk sample in the cryogenic environment creates ScS junctions. Bias current flowing through the constriction of about 10 nm in diameter exceeds the superconducting critical current value

and causes the contact area transition to the normal state; as a result, the studied ScS-contacts may be considered as conventional SnS-junctions.

The main features of the $I(V)$ curves for our ScS-contacts comprise a pronounced excess current at low bias voltages and a subharmonic gap structure (SGS) in the dI/dV curve. The latter shows sharp dips at a set of bias voltages V_n. For interpreting these dips, we use theoretical model by Kümmel et al. [2], applicable for conductance spectra of the symmetric ScS-contacts:

$$V_n = \frac{2\Delta}{en}, \quad n = 1, 2 \ldots \tag{1}$$

As the subharmonic number n increases, the dip amplitude decays. By plotting the $V_n(1/n)$ dependence (which must pass through the (0; 0) point), it is easy to determine the gap value accurately. In the case of a two-band superconductor, two distinct SGS should be observed.

Due to the local character of the Andreev spectroscopy of ScS break junctions, studies of the SGS for individual Sharvin type [11] nanocontacts allow to gain information even in case of inhomogeneous samples. In order to observe SGS, the size a of the Andreev contact should be significantly smaller than the quasiparticles mean free path l (the ballistic regime) [2–4].

Because of the layered structure of Fe-based superconductors, exfoliation of the sample generates nanosteps and terraces in the c-direction, and thus may form not only single ScS-junctions but also arrays of the S–c–S–c–…–S-type junctions. The array represents a stack of several consequently connected ballistic ScS-junctions causing an intrinsic multiple Andreev reflections effect. The latter is similar to the intrinsic Josephson effect in SIS-array [12]. Using stacks of contacts, one can exclude surface distortion of superconductivity and observe sharp peculiarities corresponding to *the true bulk gaps*. Bias voltages for these singularities should scale with the number of contacts N in the stack.

For temperatures up to T_C, the gap Δ may be obtained directly by substituting to Eq. (1) the bias voltages corresponding to the dips [2]. Our data for three different materials are shown in Figs. 1–5; they are typical for clean classical SnS-contacts [2]. As will be shown below, the data manifest two distinct sequences of dips.

The $I(V)$ and $dI(V)/dV$-characteristics were measured by a computer controlled set-up using a 16 bit National Instrument board. The dynamic conductance spectra $dI(V)/dV$ were measured by a standard modulation technique [13].

3 Experimental Results

3.1 $CeO_{1-x}F_xFeAs$

In this section, we present Andreev spectroscopy data for Ce-1111 break junctions. The results reveal the existence

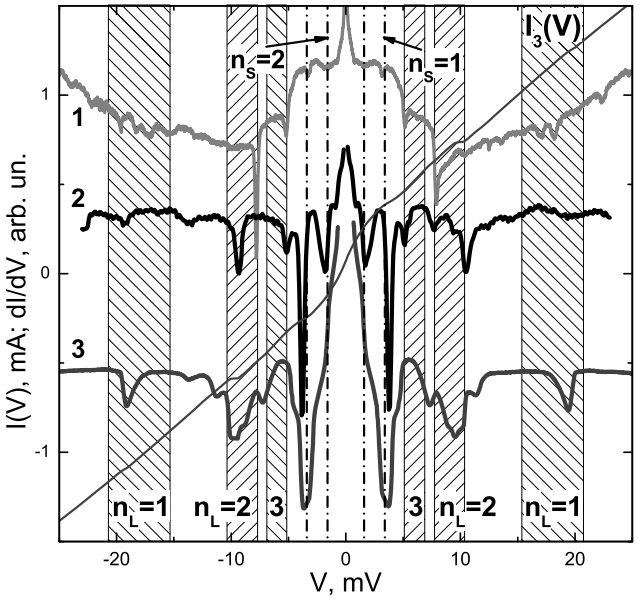

Fig. 1 Ce-1111. dI/dV-characteristics of three representative ScS–contacts at $T = 4.2$ K: sample Ce1, contacts ♯$d1$ (1) and ♯$d2$ (2), and sample Ce2, contact ♯$d6$ (3). *Thin line* $I_3(V)$ shows CVC for the latter contact. The data reveal two sets of SGS corresponding to the gaps $\Delta_L \approx 9$ meV (marked with n_L labels), and $\Delta_S \approx 1.6$ meV (*dash-dotted vertical lines* with n_S labels). *Dashed areas* cover a 15 % uncertainty for the large gap value. The *curves* are shifted vertically, for clarity

of two superconducting energy gaps and enable evaluating their magnitude at $T = 4.2$ K. To the best of our knowledge, the gap values were not measured for this material earlier. The polycrystalline $CeO_{0.88}F_{0.12}FeAs$ samples with $T_C^{\text{bulk}} \approx 41$ were synthesized as described in [14].

Dynamic conductance for three single ScS-contacts ♯$d1$, ♯$d2$ (marked as 1 and 2) for sample Ce1, and ♯$d6$ (3) for sample Ce2 is shown in Fig. 1, where one can see two sets of SGS. For comparison, the figure also shows the excess-current CVC for contact (3). The dashed areas comprise respective minima of the first set (marked with n_L labels and originating from the large gap) and represent a 15 % uncertainty. Somewhat reduced intensity of the $n_L = 1$ minima may be caused by a slight overheating of the contact area at the highest bias voltages. The fine structure in the bias voltage interval between $n_L = 1$ and $n_L = 2$ signals a large gap anisotropy of about 30 %.

The small gap SGS starts with minima located at $V_{S1} \approx \pm 3.3$ mV (marked with dash-dotted vertical lines and n_S labels), which have rather high relative amplitude, higher than the third Andreev dip from the large gap SGS. The sharp increase in the dip amplitude signals onset of a new SGS. Beyond the $n_S = 1$ dips, one can also see the $n_S = 2$ dips located at $V_{S2} \approx \pm 1.6$ mV.

The Andreev minima positions for the large and the small gap $V_{nL,S}$ are plotted in Fig. 2 as a function of $1/n$. The plot clearly demonstrates the anticipated linear dependence,

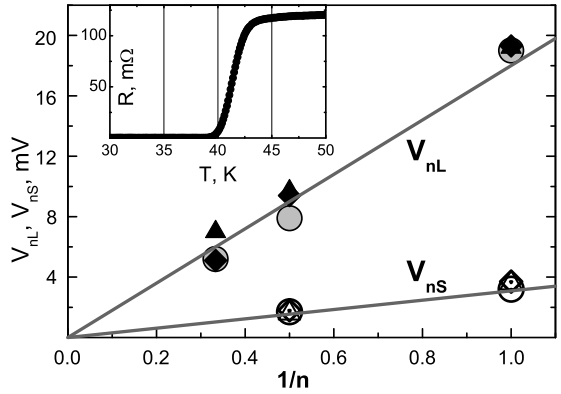

Fig. 2 Minima positions $V_{nL} = 2\Delta_L/en_L$ and $V_{nS} = 2\Delta_S/en_S$ versus $1/n$ for the studied Andreev ScS nanocontacts (see Fig. 1): sample Ce1, contacts ♯$d1$ (*circles*) and ♯$d2$ (*triangles*), and sample Ce2, contact ♯$d6$ (*rhombs*). The averaged gap values are $\Delta_L = 9.0 \pm 1.4$ meV, $\Delta_S = 1.6 \pm 0.3$ meV. *Inset* shows temperature dependence of the resistance through the superconducting transition for Ce-1111 sample ($T_C^{\text{bulk}} = 41 \pm 1$ K)

which proves unambiguously that the dips in Fig. 1 do form two independent SGS, related with the presence of two superconducting gaps. The slope of the two fitting lines gives $\Delta_L = 9.0 \pm 1.4$ meV, and $\Delta_S = 1.6 \pm 0.3$ meV, for the large and small gaps, respectively. Taking into consideration the bulk $T_C = 41 \pm 1$ K values (see inset to Fig. 2), we find the BCS ratio $2\Delta_L/k_B T_C^{\text{bulk}} \approx 5.1$ for the large gap, and $2\Delta_S/k_B T_C^{\text{bulk}} \approx 0.9$ for the small gap.

3.2 $LaO_{1-x}F_xFeAs$

We studied about 50 ScS-Andreev contacts in polycrystalline $LaO_{0.9}F_{0.1}FeAs$ (LOFA) samples with bulk $T_C^{\text{bulk}} = (28 \pm 1)$ K. The dynamic conductance $dI(V)/dV$ of single contacts and nanosteps demonstrates two well-reproducible sets of SGS corresponding to the pair of independent gap values. The number N of elementary contacts in a stack was controlled by comparing the single contact $dI(V)/dV$ spectra with those for several stacks normalized to a single junction spectrum. Figure 3 shows the $dI(V)/dV$ spectra for a single contact ♯$d17$ (black curve) and for the stacks ♯$d9$ and ♯$d10$ with various number of junctions in the array ($N = 2$, gray curve $dI_9(V)/dV$, and $N = 4$, dashed curve $dI_{10}(V)/dV$, respectively). Scaling of the SGS with properly selected number of contacts N in nanosteps is straightforward. Following the equation of Kümmel et al. [2], we easily obtain the large gap $\Delta_L \approx 6.1$ meV. As for the small gap minima, peculiarities marked by arrows (at the top of Fig. 3 and in the inset) give $\Delta_S = 0.8$ meV and 1.25 meV values at $T = 4.2$ K for the single contact ♯$d17$ and for the array ♯$d9$, respectively. By tracing the $\Delta_{L,S}(T)$ temperature dependence, we found the local critical temperature of the contact area T_C^{local}. The values obtained, $\Delta_L \approx 6.1$ meV,

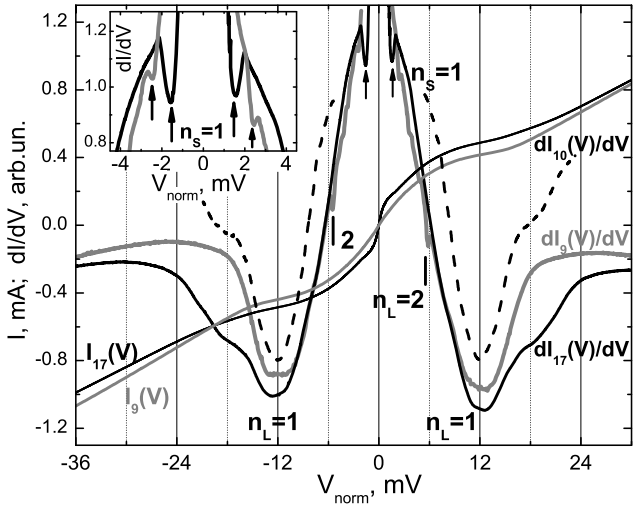

Fig. 3 La-1111. Normalized CVC and dynamic conductance of Andreev contacts for sample LOFA5: contacts ♯$d10$ ($N = 4$ junctions in a stack, *dashed line*), ♯$d9$ ($N = 2$, *gray lines*), both normalized to ♯$d17$ (single junction, *black lines*). $T_C^{\text{local}} \approx 26$ K. The SGS for the large gap (n_L labels) gives $\Delta_L \approx 6.1$ meV for all the contacts, the small gap $\Delta_S \approx 0.8$ meV (contact ♯$d17$) and 1.25 meV (contact ♯$d9$) SGSs are marked by *black arrows* and n_S labels. *Inset* blows-up details of the small gap SGS for contacts ♯$d17$ and ♯$d9$

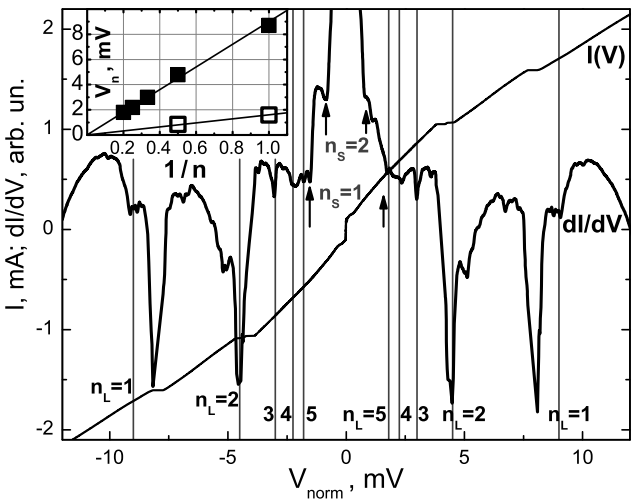

Fig. 4 La-1111. Normalized CVC and dynamic conductance of a two–contact Andreev array. The SGS of the large gap (n_L labels) gives $\Delta_L \approx 4.5$ meV ($T_C^{\text{local}} \approx 25$ K). *Thin vertical lines* represent the expected location of Andreev minima in accordance with theoretical formula $V_n = 2\Delta/en$ from [2]. The set of small gap peculiarities (n_S labels and *black arrows*) lead to $\Delta_S \approx 0.8$ meV. (*Inset*) The $V_n(1/n)$ dependences plotted for the SGS minima of both gaps (using the data from the main panel). *Lines* average the experimental values

$\Delta_S \approx 1.25$ meV, and $T_C^{\text{local}} = 26 \pm 1$ K are close to the results of [15].

Figure 4 shows normalized CVC and dynamic conductance of two-contact ScS-Andreev array ♯$d14$ in another LaO(F)FeAs sample. The sharp SGS related to the large

gap (marked with n_L labels) gives $\Delta_L \approx 4.5$ meV (see solid squares in the inset to Fig. 4). Interestingly, all these Andreev minima up to $n_L = 5$ are double-split. It seems that the doublets observed on the high-quality characteristics are caused by some anisotropy of the Δ_L order parameter, though it has no nodes, as was shown in [6]. The CVC shown in Fig. 4 demonstrates a small Josephson supercurrent at zero bias caused by the tunneling between the sample clefts. An SGS associated with the small gap (n_S labels and arrows) leads to $\Delta_S \approx 0.8$ meV value (see open squares in the inset to Fig. 4).

The BCS-ratio $2\Delta_L/k_BT_C^{\text{local}} = (4.2 \div 5.6)$ exceeds the standard value 3.52 and thus is in favor of a strong coupling in the Δ_L condensate. At the same time, the small value, $2\Delta_S/k_BT_C^{\text{local}} < 1.2$, is a result of induced superconductivity at finite temperatures in the bands with the small gap. These values support data reported earlier in [6] and are in close agreement with the experimental results on GdO(F)FeAs [7] and our data on MgB_2 [16, 18].

3.3 FeSe

Among the new class of Fe-based superconductors [9], layered FeSe has the simplest crystal structure and relatively low critical temperature T_C. Polycrystalline FeSe samples have been grown from melt by spontaneous nucleation. The synthesis process was described in detail in [8]. The intrinsic multiple Andreev reflections effect was observed in FeSe nanosteps earlier [8].

The $I(V)$ and $dI(V)/dV$ characteristics for several ScS-junctions formed by successive mechanical readjustments of the contact are shown in Fig. 5. Two sets of SGS with a number of dips are clearly seen. The first set of dips (n_L labels) gives the large gap value $\Delta_L \approx 2.6$ meV. The second set of dips (n_S labels) corresponds to the small gap $\Delta_S \approx 1$ meV. It is worth noting that the dip positions and, consequently, the gap values remain unchanged under the readjustment of the contact. This proves the high homogeneity of the sample superconducting properties in the contact area. The superconducting gap values at $T = 4.2$ K averaged over more than 30 ScS-contacts, are $\Delta_L = 2.8 \pm 0.4$ meV and $\Delta_S = 0.8 \pm 0.2$ meV ($T_C^{\text{bulk}} = 12 \pm 1$ K). These results agree with the preliminary data obtained with similar samples [8].

Figure 6 shows the $\Delta_{L,S}(T)$ temperature dependences for two ScS-contacts in FeSe. For the large gap, the $\Delta_L(T)$-curve lies slightly below the standard BCS-like dependence. For the small gap, the $\Delta_S(T)$ dependence deviates essentially from the BCS-type curve and is in a good agreement with the calculations in [17]. Knowing the local $T_C^{\text{local}} \approx 9.7$ K, one can calculate the BCS-ratio. For the large gap, we obtain $2\Delta_L/k_BT_C^{\text{local}} \approx 5.7$ which exceeds the BCS value for a single-gap superconductor. On the other hand, for the small gap, the $2\Delta_S/k_BT_C$ ratio is much smaller than 3.52. Such a behavior resembles the situation in MgB_2 [18–20] and, by parity of reasoning, can be explained by the k-space proximity effect [21, 22] between two superconducting condensates, where the large gap condensate plays a "driving" role.

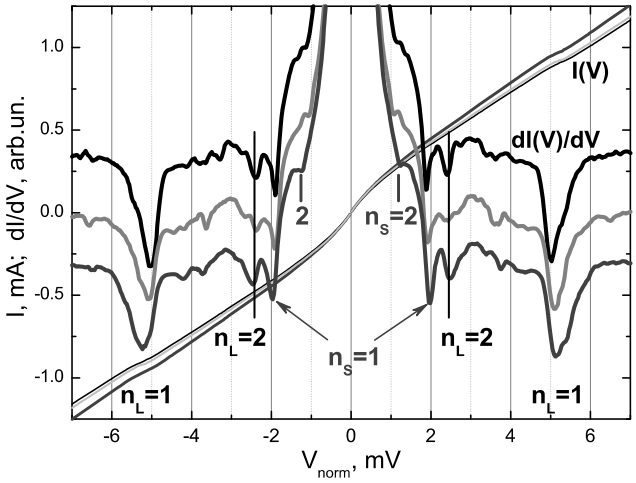

Fig. 5 FeSe. Normalized to a single junction CVC and dI/dV spectra for ScS-Andreev contacts (sample FS1, contacts ♯$d8$, ♯$d9$, ♯$d11$ of three SnS-junctions in a stack; $T_C = 12.5$ K, $T = 4.2$ K). Two SGS at bias voltages $V_{nL,S} = 2\Delta/en_{L,S}$ corresponding to the large (n_L labels) and the small gap (n_S labels) yield $\Delta_L \approx 2.6$ meV and $\Delta_S \approx 1$ meV values

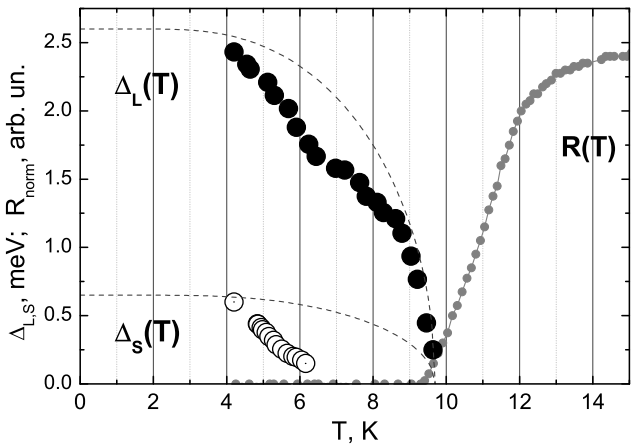

Fig. 6 Temperature dependence of two superconducting gaps $\Delta_L(T)$ for FeSe (sample FS1, contact ♯b; $\Delta_L(4.2\text{ K}) = 2.4 \pm 0.2$ meV) and $\Delta_S(T)$ (sample FS2, contact ♯b; $\Delta_S(4.2\text{ K}) = 0.7 \pm 0.1$ meV). Local $T_C^{\text{local}} = 9.7 \pm 0.5$ K. Single-gap BCS-like curves (*dashed lines*), and the sample resistance $R_{\text{norm}}(T)$ are shown for comparison

4 Discussion

It was pointed out [23] that inelastic neutron scattering data can provide valuable information about the symmetry of the

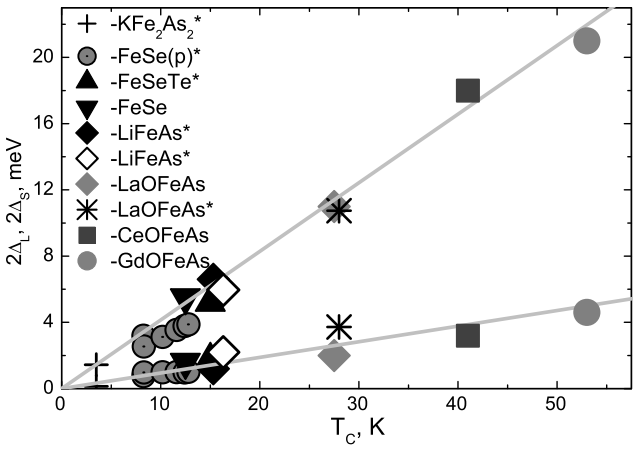

Fig. 7 Scaling of the superconducting gap values with T_C for iron-based superconductors: $2\Delta_L/k_BT_C = 4.8 \pm 1.0$ and $2\Delta_S/k_BT_C = 1.1 \pm 0.4$. *Asterisks* mark the data obtained by other groups (see Refs. in [8])

superconducting gap in novel superconductors. Calculations showed, in particular, that a hump structure must appear in the dynamic spin susceptibility just above the 2Δ energy in the case of an s^{++} wave state (the fully gapped s-wave state without sign reversal) [23]. Recently, the experimental linear dependence of the spin resonance energy $E_{\rm res}$ on T_C with the average slope $4.7k_BT_C$ was found for several iron based superconductors (see, e.g., Fig. 5 in [24]). Within experimental errors, this dependence coincides with our plot (Fig. 7) of the superconducting gap $2\Delta_L$ *versus* T_C *for several* iron based superconductors: Ce-1111 (present measurements), FeSe [8], LaO(F)FeAs [6], GdO(F)FeAs [7], as well as KFe_2As_2, $FeTe_{1-x}Se_x$, LiFeAs, (see Fig. 11 in [8] and references therein). Although the scattering of data in Fig. 7 is quite significant, two linear dependencies emerge with $2\Delta_L/k_BT_C = 4.8 \pm 1.0$ and $2\Delta_S/k_BT_C = 1.1 \pm 0.4$. The coincidence of $2\Delta_L/k_BT_C$ (Fig. 7) and $E_{\rm res}/k_BT_C$ (Fig. 5 in [24]) supports the version of a fully gapped s-wave state without sign reversal [23].

In conclusion, we studied properties of CeO(F)FeAs, LaO(F)FeAs, and FeSe superconductors by ScS-Andreev- and IMARE spectroscopies. The dynamic conductance curves for single and stack ScS-contacts cannot be described within the single-gap framework and evidence for the two-gap superconductivity in these compounds. For the first time studied CeO(F)FeAs ($T_C^{\rm bulk} \approx 41$ K), we determined the two superconducting gaps $\Delta_L = 9.0 \pm 1.4$ meV, and $\Delta_S = 1.6 \pm 0.3$ meV; the respective BCS-ratios are $2\Delta_L/k_BT_C^{\rm bulk} \approx 5.1$, and $2\Delta_S/k_BT_C^{\rm bulk} \approx 0.9$.

For LaO(F)FeAs ($T_C^{\rm bulk} \approx 28$ K), we also determined the two superconducting gap values $\Delta_L = 4.5 \div 6.5$ meV, $\Delta_S = 0.8 \div 1.3$ meV, leading to the BCS-ratios $2\Delta_L/k_BT_C^{\rm local} = 4.2 \div 5.6$ and $2\Delta_S/k_BT_C^{\rm local} = 0.6 \div 1.2$, respectively ($T_C^{\rm local} = 25 \div 29$ K). We observed splitting of the SGS dips for high-quality characteristics, suggestive of an anisotropy of the Δ_L order parameter.

For FeSe ($T_C^{\rm bulk} \approx 12$ K), our IMARE spectroscopy data point to $\Delta_L = 2.8 \pm 0.4$ meV, $\Delta_S = 0.8 \pm 0.2$ meV, and $2\Delta_L/k_BT_C^{\rm local} \approx 5.7$, $2\Delta_S/k_BT_C^{\rm local} \approx 1.5$. The temperature dependences $\Delta_{L,S}(T)$ indicate the k-space proximity effect between two superconducting condensates. The large gap BCS-ratio for all the materials studied exceeds 3.52, indicating a strong electron-boson coupling in the "driving" large gap condensate. The BCS-ratio for the small gap appears to be much less than 3.52, thus suggesting an induced superconductivity at finite temperatures in the "driven" Δ_S condensate due to a nonzero interband coupling. Finally, our data confirm a linear relation between the superconducting gap Δ_L and magnetic resonance energy $E_{\rm res} \approx 2\Delta_L$, valid for various Fe-based superconductors.

Acknowledgements The work was supported by the Russian Ministry of Education and Sciences (contract 11.519.11.60.12, grant 8375), RFBR (grants 12-02-31269, 13-02-01451), DFG Grants 436RUS113 and FOR 538/BU887/4, and DFG priority program (SPP1458). We thank T. Hänke, C. Hess, G. Behr, R. Klingeler, and B. Büchner for the La-1111 samples synthesis.

References

1. Andreev, A.F.: Sov. Phys. JETP **19**, 1228 (1964)
2. Kümmel, R., et al.: Phys. Rev. B **42**, 3992 (1990)
3. Poenicke, A., et al.: Phys. Rev. B **65**, 220510 (2002)
4. Blonder, G.E., et al.: Phys. Rev. B **25**, 4515 (1982)
5. Seidel, P.: Supercond. Sci. Technol. **24**, 043001 (2011)
6. Ponomarev, Ya.G., et al.: Phys. Rev. B **79**, 224517 (2009)
7. Shanygina, T.E., et al.: JETP Lett. **93**, 94 (2011)
8. Ponomarev, Ya.G., et al.: J. Exp. Theor. Phys. **113**, 459 (2011)
9. Kamihara, Y., et al.: J. Am. Chem. Soc. **130**, 3296 (2008)
10. Moreland, J., Ekin, J.W.: J. Appl. Phys. **58**, 3888 (1985)
11. Sharvin, Yu.V.: Zh. Eksp. Teor. Fiz. **48**, 984 (1965)
12. Nakamura, H., et al.: J. Phys. Soc. Jpn. **78**, 123712 (2009)
13. Ponomarev, Ya.G., Rakhmanina, A.V.: Prib. Teh. Eksp. **5**, 120 (1970)
14. Khlybov, E.P., et al.: JETP Lett. **90** (2009)
15. Yashima, M., et al.: J. Phys. Soc. Jpn. **78**, 103702 (2009)
16. Ponomarev, Ya.G., et al.: Solid State Commun. **129**, 85 (2004)
17. Khasanov, R., et al.: Phys. Rev. Lett. **104**, 087004 (2010)
18. Ponomarev, Ya.G., et al.: JETP Lett. **79**, 484 (2004)
19. Kuzmichev, S.A., et al.: Solid State Commun. **152**, 119 (2012)
20. Nicol, E.J., Carbotte, J.P.: Phys. Rev. B **71**, 054501 (2005)
21. Golubov, A.A., et al.: Phys. Rev. B **51**, 1073 (1995)
22. Yanson, I.K., et al.: Phys. Rev. B **67**, 024517 (2003)
23. Onari, S., et al.: Phys. Rev. B **81**, 060504 (2010)
24. Shamoto, S.-i., et al.: Phys. Rev. B **82**, 172508 (2010)